

Vehicle System Dynamics



International Journal of Vehicle Mechanics and Mobility

ISSN: (Print) (Online) Journal homepage: www.tandfonline.com/journals/nvsd20

Quantification of energy losses in suspension dampers and its effects on rolling resistance

C. J. J. Beckers, I. J. M. Besselink & H. Nijmeijer

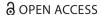
To cite this article: C. J. J. Beckers, I. J. M. Besselink & H. Nijmeijer (01 Apr 2025): Quantification of energy losses in suspension dampers and its effects on rolling resistance, Vehicle System Dynamics, DOI: 10.1080/00423114.2025.2482038

To link to this article: https://doi.org/10.1080/00423114.2025.2482038

9	© 2025 The Author(s). Published by Informa UK Limited, trading as Taylor & Francis Group.
	Published online: 01 Apr 2025.
	Submit your article to this journal $oldsymbol{\mathbb{Z}}$
ılıl	Article views: 168
a a	View related articles 🗗
CrossMark	View Crossmark data ☑









Quantification of energy losses in suspension dampers and its effects on rolling resistance

C. J. J. Beckers^{a,b}, I. J. M. Besselink^a and H. Nijmeijer^a

^aDepartment of Mechanical Engineering, Eindhoven University of Technology, Eindhoven, The Netherlands; ^bPowertrains Department, Netherlands Organisation for Applied Scientific Research (TNO), Helmond, The Netherlands

ABSTRACT

The energy consumption of battery electric buses, and electric vehicles in general, depends to a large extent on rolling resistance. Although often aggregated into one, the energy lost due to rolling resistance can be subdivided into losses occurring in or at the tyre and losses occurring in the shock absorbers of the vehicle suspension. In this paper, the energy dissipated by the dampers of a battery electric bus is quantified in an energy consumption context. The analysis is based on a description of the vertical vehicle dynamics using a quarter-car model with a nonlinear dashpot. The model is validated by comparing suspension deflection with a measurement on a known road surface. It is shown that 73% of the energy dissipated in the dampers occurs at road frequencies between 3 and 12 Hz. Model simulations on different simulated ISO 8608 road surfaces reveal that damper losses are in the order of 100 W on smooth roads (classes A and B), yet can reach values of several kW's on rough roads (class D) at 40 km/h. A comparison with rolling resistance coefficients obtained from coast-down tests shows that the damper losses can explain the majority of the rolling resistance difference between road surfaces with a different roughness.

ARTICLE HISTORY

Received 17 December 2024 Revised 7 March 2025 Accepted 12 March 2025

KEYWORDS

Vertical vehicle dynamics; nonlinear damper: rolling resistance; road roughness; energy consumption; electric buses

1. Introduction

In an effort to electrify inner-city transport, battery electric buses (BEBs) are becoming the standard ever more city centres around the world [1]. These vehicles offer reduced noise and local pollution without the cost and maintenance of overhead power lines. However, similar to electric passenger cars, the driving range of BEBs is smaller compared to Internal Combustion Engine (ICE) vehicles. This has re-ignited the interest in models that can simulate and predict the energy consumed by road vehicles.

A physics-based approach to this energy consumption analysis involves modelling the individual longitudinal forces acting on the vehicle; rolling resistance, aerodynamic resistance, slope resistance, the force accelerating the vehicle, and the powertrain losses. The rolling resistance is responsible for up to 30% of the energy consumption of a BEB [2] and is often modelled as a constant coefficient multiplied by the vertical tyre force. In reality, the



on which this article has been published allow the posting of the Accepted Manuscript in a repository by the author(s) or with their consent.

rolling resistance is a consequence of different physical mechanisms, including hysteresis losses due to the repeated deformation of the tyre tread and tyre slip. This effect is already studied extensively for bus and truck tyres [3,4]. This paper focuses on the contribution of road irregularities to the rolling resistance of heavy-duty vehicles.

1.1. Literature review

The relation between the power required to move a vehicle forward and suspension shock absorbers precedes the introduction of modern electric vehicles. At the beginning of the 1980s, road roughness was a topic of interest [5], and the link between fuel consumption and suspension stroking was made by various authors [6–8]. According to these sources, there are four mechanisms associated with vertical vehicle dynamics that contribute to additional energy losses:

- (1) Stroking of the suspension dampers
- (2) Dynamic deflection of the visco-elastic tyre, including obstacle enveloping
- (3) Impact between tyre and road [9]
- (4) Micro slip associated with angular accelerations of the wheel due to a varying effective tyre radius under dynamic wheel load [9].

Since the loss of contact between tyre and road is assumed to be unlikely on paved roads where BEBs drive, and the energy effects of item 4. are shown to be negligible at constant speed [9], only mechanisms 1. and 2. are considered in this study.

To the authors' knowledge, suspension losses are first studied in [6], using a massspring-damper model. Later, a complete analysis of the entire tyre-wheel-suspension system is presented in [8]. The latter study includes a radial spring-damper tyre model and performs analyses for realistic road inputs. This model is later extended to include loss of tyre-road contact and is compared to drum tests in [10]. In the 1990s, the observation that dampers dissipate energy led to the idea that active dampers could be used to harvest part of the energy that usually would be dissipated [11,12]. Furthermore, simulation studies have been done that employ quarter-car (QC) models to quantify damper losses, such as [13], and, more ore recently, [14]. The latter study employs a half-car model with a carefully constructed input road profile to quantify the damper losses relative to the longitudinal slip losses, also in transient conditions. Although very insightful, these studies are often performed without comparing the result to measurement data.

Most of these earlier studies employ linear quarter-car models in combination with various tyre models. However, it is established that automotive shock absorbers have nonlinear characteristics [15,16]. A linearised damper only achieves comparable results to nonlinear dampers for constant excitation amplitudes [17]. Therefore, when analyzing a variety of road roughnesses, a nonlinear damper model is required.

Damper losses are not always considered when discussing rolling resistance. Detailed empirical and finite element models exist that aim to model the resistance experienced by an individual rolling tyre [4,18-20]. The tyre models in these studies that only concern the tyre are often compared with measurements from a tyre-test setup.

The rolling resistance can also be studied using empirical methods. These studies often focus on estimating the rolling resistance coefficient based on data without considering the details of the physical mechanisms through which energy is dissipated, such as the subdivision between losses in tyre or suspension. Huang and Chen [21] and Ejsmont et al. [22] are examples of empirical models for the rolling resistance of truck tyres based on tyre measurements. The resulting models describe a statistical relation between the rolling resistance coefficient and the road roughness, typically indicated by Mean Profile Depth (MPD) or International Roughness Index (IRI). Other studies directly relate the road roughness to fuel consumption through regression analysis [23], without considering the rolling resistance coefficient in detail. While these empirical methods work well if ample data is available of the vehicle and road of interest, extrapolation to unobserved situations can prove difficult. In contrast, a physics-based model of the suspension would open the door towards energy predictions on road types on which the vehicle has not yet driven.

1.2. Contribution

This paper presents a quantitative analysis of the energy dissipated in the suspension dampers due to road irregularities and evaluates the results in an energy-consumption context. This study focuses on the interplay between vehicle modelling, damper modelling, and road roughness modelling by providing a quantitative analysis using relatively simple models, considering the often limited data available. By matching the model complexity of all parts of the system, i.e. suspension, tyre, and road, this study provides a qualitative analysis of each part towards energy consumption.

The contributions of this paper are threefold: First, a quarter-car model with nonlinear suspension damper characteristics is validated by comparison to multiple vehicle tests. Secondly, to support this validation, road-profile measurements are augmented with data from a Digital Elevation Model (DEM) to arrive at an accurate road description over a wide frequency range. Lastly, using the validated nonlinear quarter-car model, the energy dissipated in the dampers of a BEB is quantified for different road conditions and is compared to experimentally determined rolling resistance coefficients. The methods presented are generally applicable and allow subdivision of the rolling resistance into damper losses and tyre losses. The method is demonstrated using specific vehicle parameters to quantify the results and demonstrate the relevance of the considered effects.

This paper is organised as follows. In Section 2 a quarter-car model is presented to describe the vertical dynamics of a battery electric city bus. Model validations are provided in Section 3 using experimental data recorded on two different road surfaces. In Section 4 the validated quarter-car model is used to quantify the damper losses in the suspension of a battery electric bus. The results are compared to coast-down tests conducted with a similar vehicle. Lastly, in Section 5, the conclusions of the work are summarised, and the prospects of future work are discussed.

2. Quarter-car vehicle model

An often employed model in vehicle dynamics literature is the quarter-car model [24, p. 194-196]. This model describes the vertical displacement of one corner of the vehicle, with sprung mass m_s and unsprung mass m_u , as visualised in Figure 1. Both masses are subject to the gravitational acceleration g and are interconnected by a spring with stiffness k_s and, in this case, a nonlinear damper. The unsprung mass m_u is connected to the

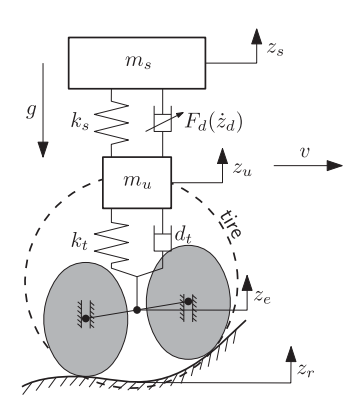


Figure 1. Schematic view of the quarter-car model with a nonlinear spring, a nonlinear damper, and a tandem-cam enveloping model.

road via the tyre, represented by a linear spring with stiffness k_t and a linear damper with damping constant d_t . The tyre-road contact is modelled using a tandem model with elliptical cams according to [25, Chapter 4]. Two cams, a longitudinal distance apart, follow the road profile z_r , thereby simulating the enveloping of small objects by the tyre and generating an effective road profile z_e that is perceived by the quarter-car model. The model does not include the rolling resistance due to hysteric tyre losses.

The model features a nonlinear damper, where the damper force $F_d(\dot{z}_d)$ is a function of the suspension deflection rate \dot{z}_d , with

$$\dot{z}_d = \dot{z}_s - \dot{z}_u. \tag{1}$$

Automotive shock absorbers generally have a nonlinear characteristic, with damper forces that are typically larger during extension than during compression [15,16]. This damper characteristic is realised passively using a series of internal chambers, orifices, and check valves through which hydraulic oil can flow. Secondly, linear tyre damping d_t , although small compared to suspension damping, is included here because it contributes to the total energy dissipated in the system.

Based on Figure 1, the following equations of motion can be defined for the quarter-car model;

$$m_s \ddot{z}_s = -k_s (z_s - z_u) - F_d(\dot{z}_d) - m_s g,$$

$$m_u \ddot{z}_u = -k_t (z_u - z_e) + k_s (z_s - z_u) - d_t (\dot{z}_u - \dot{z}_e) + F_d(\dot{z}_d) - m_u g.$$
 (2)

These two second-order differential equations are rewritten to a system of first-order differential equations by defining the state column x(t) and input column u(t) according to:

$$x(t) := \begin{bmatrix} \dot{z}_s & \dot{z}_u & z_s & z_u \end{bmatrix}^\top \qquad u(t) := \begin{bmatrix} \dot{z}_e & z_e \end{bmatrix}^\top. \tag{3}$$

In contrast to a quarter-car model without tyre damping, the input column includes the time derivative of the effective road height \dot{z}_e , which is required to calculate the tyre damping force. Using the definitions in (3), (2) can be written as a first-order ordinary differential

equation:

$$\dot{x}(t) = f(x(t), u(t)) \tag{4}$$

with

$$f(x(t), u(t)) = \frac{1}{m_s} \left(-F_d(x_1 - x_2) + k_s x_4 - k_s x_3 \right) - g$$

$$\left[\frac{1}{m_u} \left(F_d(x_1 - x_2) - (k_t + k_s) x_4 + k_s x_3 - d_t x_2 + d_t u_1 + k_t u_2 \right) - g \right]. \tag{5}$$

$$x_1$$

$$x_2$$

To perform the simulations presented in this paper, the system of equations described by (4) is implemented in Simulink and integrated with respect to time using an explicit numerical solver; in this case MATLAB's ode3 [26], with a fixed time step of 1 ms. A fixedstep solver is used here because an equidistant time vector will allow easy analysis of the model outputs in the frequency domain later. At the start of every simulation, the system is assumed to be at rest. This implies that all time derivatives are zero and the initial positions represent the static deflections of suspension and tyre due to gravity, with the road height z_r being equal to zero:

$$x(t=0) = \begin{bmatrix} 0 & 0 & -\frac{m_s g}{k_s} - \frac{(m_s + m_u)g}{k_t} & -\frac{(m_s + m_u)g}{k_t} \end{bmatrix}^{\top}.$$
 (6)

2.1. Air suspension characteristics

Most modern battery electric buses are equipped with Electronically Controlled Air Suspension (ECAS). This system keeps the ride height approximately constant under varying passenger occupancy conditions and allows the vehicle to 'kneel' at bus stops by lowering one side of the vehicle. The used airbellows poses a slightly progressive force-displacement characteristic, which is also a function of the bellow pressure. In this work, the air bellow is modelled as a quasi-linear spring with stiffness $k_{b,lin}$, which is based on the airbellow specifications and depends linearly on the static bellow pressure $p_{b,stat}$ and thus on the sprung mass m_s :

$$k_s = n_h k_{h,lin}(p_{h,stat}(m_s)), \tag{7}$$

where n_b is the number of bellows per vehicle corner. The used stiffness values are mentioned respectively in Tables 1 and 2. This linear-spring approach keeps the model relatively simple, while still taking into account the most important effects for energy consumption. Particular to ECAS is that, due to the m_s -dependency of k_s , the sprung mass resonance frequency remains approximately constant for changing sprung masses. Any damping or hysteresis that the air bellow provides is assumed to be negligible compared to the damping force of the hydraulic shock absorbers.

Table 1. Model parameters of the quarter-car model that represents the vehicle used in the validation tests.

Parameter	Symbol	Value	Unit
Sprung mass (unladen)	m _{s.unlad}	1310	kg
Sprung mass (laden)	$m_{s,lad}$	3042	kg
Unsprung mass	m _u	600	kg
Bellow stiffness (unladen)	k _{s,unlad}	92000	N/m
Bellow stiffness (laden)	k _{s,lad}	154000	N/m
Damper force	$F_d(\dot{z}_d)$	Figure 2	N
Tyre stiffness	k _t	2.3 · 10 ⁶	N/m
Tyre damping	d_t	600	Ns/m

Table 2. Model parameters of the quarter-car models that represent the front and rear axle of a battery electric bus.

Parameter	Symbol	Value Front Axle	Value Rear Axle	Unit
Sprung mass (unladen)	m _{s.unlad}	2390	3685	kg
Sprung mass (laden)	$m_{s,lad}$	3018	5037	kg
Unsprung mass	m_u	425	695.5	kg
Bellow stiffness (unladen)	k _{s,unlad}	151000	175000	N/m
Bellow stiffness (laden)	k _{s.lad}	182000	236000	N/m
Damper force	$F_d(\dot{z}_d)$	Figure 10(a)	Figure 10(b)	N
Tyre stiffness	k_t	1.15 · 10 ⁶	2.3 · 10 ⁶	N/m
Tyre damping	d_t	300	600	Ns/m

3. Model validation

In this section, two experiments are discussed that compare the output of the quartercar model to measured suspension deflections. First, the specific vehicle used for these validation tests is described in Section 3.1. Next, Sections 3.2 and 3.3 describe experiments where the vehicle is driven over a specific road, and the suspension deflection is compared to the quarter car simulation results.

3.1. Vehicle parameters

An articulated, three-axle, 18 m diesel bus is used for the validation experiments. Even though the vehicle has no electric powertrain, the suspension and chassis are similar to that of a battery electric bus, with the exception of a higher vehicle mass. The second axle of the vehicle is considered. This is a non-driven, non-steered axle with two air bellows, two dampers, and two tyres per corner of the vehicle. The vehicle is instrumented with potentiometers parallel to each of the four dampers of the axle. The used sensors are of type ASM® WS10P-375-MCANOP-L10-SB0-M12. This allows for measurement of the damper deflection z_d with an accuracy of 0.2 mm at a sampling rate of 500 Hz during normal operation of the vehicle. Signals were recorded with an $\mbox{IMC}^{\mbox{\scriptsize (B)}}$ instruments BUSDAQ2.

The parameters of the quarter-car model simulating this vehicle are listed in Table 1. The damper and spring characteristics originate from the respective manufacturer information, except for the vertical tyre damping, which is taken from [27]. The unsprung mass originates from component specifications of the axle and tyres, and the sprung masses for

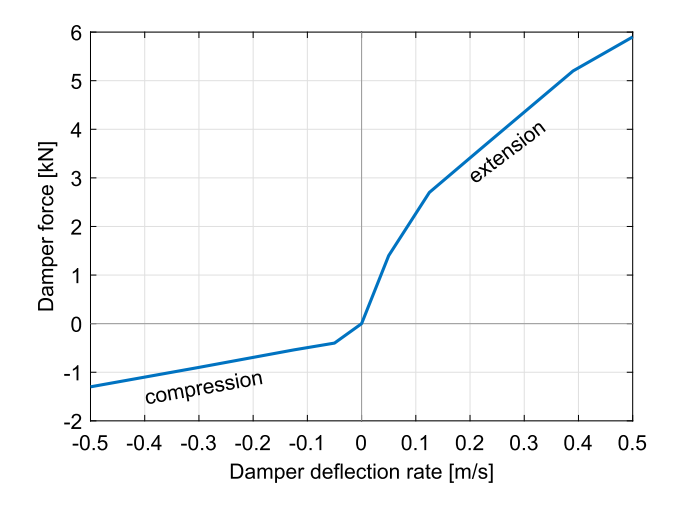


Figure 2. Damper force F_d versus damper deflection rate \dot{z}_s for the vehicle used in the validation tests. Values represent two dampers combined, as would occur on one corner of the second axle of a vehicle. Data according to manufacturer specification.

both a laden and an unladen vehicle are determined by measurements. Because the air bellow stiffness depends on the sprung mass according to (7), this parameter is also reported for both loading conditions. Enveloping model parameters for a 245/75 R16 tyre are taken from [25, Table 4.4], because these are geometrically closest to a bus tyre.

The force $F_d(\dot{z}_d)$ for this axle is visualised in Figure 2. This is the combined force of two dampers that act in parallel. The damper characteristic shows that the damping force is approximately a factor five higher for extension than for compression at equal deflection rates.

3.2. Road bump test

In a first test, the laden vehicle is driven with a constant velocity of 30 km/h over a well-defined obstacle. The road section of interest is a bump with a relatively steep increase and a more gradual decrease, as is displayed in Figure 3. The bump is measured and subsequently modelled using a piecewise affine road-height profile.

The results of the measurement are presented in Figure 4, together with the simulated deflection from the quarter-car model. The instance the second axle of the vehicle encounters the bump is visible in the figure as t_1 , and after this moment, the suspension is compressed 60 mm. The axle reaches the top of the bump at t_2 , after which the rebound of the suspension occurs and the dampers extend to approximately -80 mm. The results show that the quarter-car model accurately simulates this initial compression and the subsequent rebound. At t_3 , the third axle of the vehicle encounters the bump. After this moment, the simulation and measurement no longer coincide because the load transfer between different axles is not included in the simulation. Nevertheless, from the data in the range $t = [t_1 \ t_3]$ it can be concluded that the model matches the measurements well. The RMS error of the suspension deflection is 17 mm, which is small compared to the total deflection of approximately 150 mm.

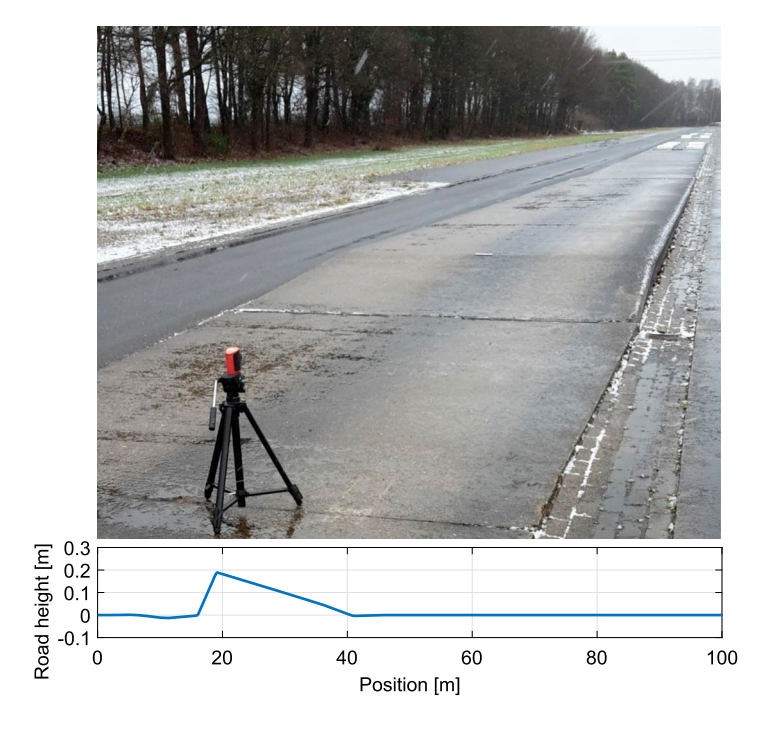


Figure 3. Photo of the road bump with a laser sensor (top) and the modelled road height z_r of the road bump as function of position x (bottom).

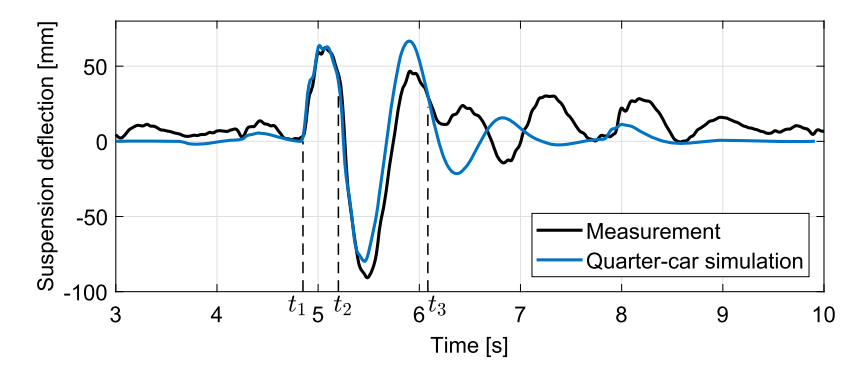


Figure 4. Measured and simulated suspension travel of the second axle. Time instances t_1 , t_2 , and t_3 respectively indicate the start of the bump, the top of the bump, and the instance the third axle encounters the start of the bump.

3.2.1. Energy decomposition

After simulating the road bump, the full state of the system x(t) is known for all time instances. This information can subsequently be used to construct the system's energy balance. Firstly, the kinetic energy is calculated as

$$E_{kin}(t) = \frac{1}{2} m_s \dot{z}_s^2(t) + \frac{1}{2} m_u \dot{z}_u^2(t).$$
 (8)

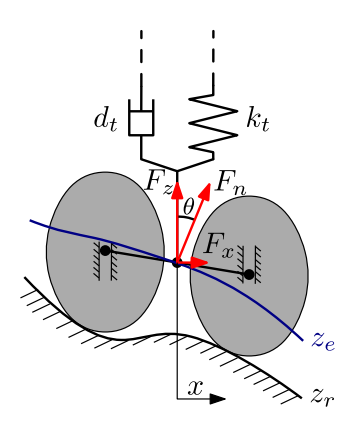


Figure 5. Schematic view of the tyre-road contact point with the effective road profile z_e indicated in blue, and forces indicated in red.

Secondly, the potential energy of the system equals

$$E_{pot}(t) = \frac{1}{2}k_s (z_s(t) - z_u(t))^2 + \frac{1}{2}k_t (z_u(t) - z_e(t))^2 + m_s z_s(t)g + m_u z_u(t)g.$$
 (9)

Lastly, the energy dissipated due to non-conservative forces acting on the system is calculated according to

$$E_{dis}(t) = E_{damp}(t) + E_{tyr}(t) = \int_{\tau=0}^{t} F_d(\dot{z}_d(\tau)) \cdot \dot{z}_d(\tau) d\tau + \int_{\tau=0}^{t} d_t (\dot{z}_u(\tau) - \dot{z}_e(\tau))^2 d\tau.$$
(10)

According to the conservation of energy, the sum of these energies ΣE should be equal to the work exerted on the system W:

$$\Sigma E(t) = E_{kin}(t) + E_{pot}(t) + E_{dis}(t) = W(t). \tag{11}$$

This work is derived by examining the tyre-road contact point, as detailed in Figure 5. The modelled contact exerts a normal force F_n on the vehicle, which is decomposed in a vertical dynamic tyre force F_z and a longitudinal force F_x . If the vehicle is moved at a constant longitudinal velocity, this force F_x exerts work on the system, which can be calculated according to:

$$W(t) = \int F_x(t) dx \quad \text{with} \quad F_x(t) = F_z(t) \tan(\theta(t)), \tag{12}$$

where $\theta(t) = -\arctan(dz_e(t)/dx)$ and F_z is the dynamic tyre force, which can be calculated according to

$$F_z(t) = -k_t (z_u(t) - z_e(t)) - d_t (\dot{z}_u(t) - \dot{z}_e(t)).$$
(13)

The potential-, kinetic- and dissipated energy resulting from the bump simulation are visualised in Figure 6. At the start of the simulation, the system is in its initial position, and the internal energy is zero. At t_1 , the axle encounters the bump, resulting in an increase of the potential energy E_{pot} first and then also of the kinetic energy E_{kin} . Note that the energy dissipated in the dampers is still low at this point. Only after t_2 , when the axle has reached

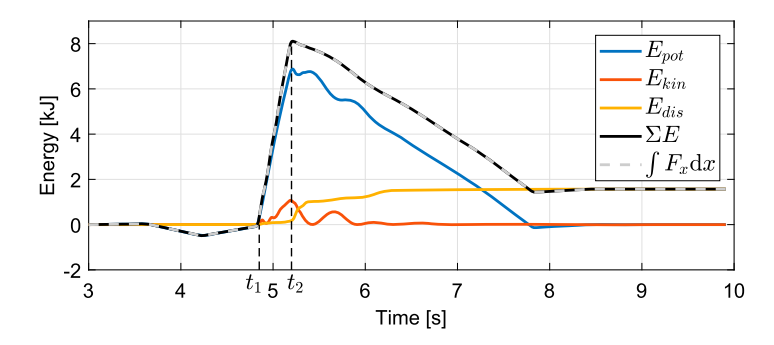


Figure 6. Energy decomposition of the bump simulation. Time instances t_1 and t_2 respectively indicate the start and top of the bump.

the top of the bump and the rebound starts, most energy is dissipated. The oscillations in E_{pot} and E_{kin} disappear again, and, at the end of the simulation, both are zero. In contrast, E_{dis} is non-zero at the end, indicating that 1.8 kJ was dissipated in the tyre and the damper. The majority of this dissipation happens during the rebound, just after t_2 . Lastly, simulated values for $\Sigma E(t)$ and $\int F_x dx$ show the conservation of energy in the model.

3.3. Belgian blocks test

In the second test, the vehicle is driven over several strips of Belgian blocks. This specific road has been designed to represent a worst-case situation regarding the loading of the suspension and is generally used in durability tests. The measured section consists of two strips of Belgian blocks, one with a length of 306 m and one of 714 m, connected by a section of smooth asphalt. These strips are traversed at a constant velocity of $v = 40 \,\mathrm{km/h}$ using the vehicle described in Section 3.1, resulting in a measurement with a duration of approximately 100 s.

3.3.1. Simulated road input

To simulate a stretch of Belgian blocks, information on the road height z_r is required. Because the road considered is part of a test track, a profile of the Belgian-block section is available. The frequency content of the road height is visualised in Figure 7. The road classes according to ISO 8608 [28] are also indicated in the figure and show that the Belgian-block road is of class D or E for the higher frequencies. However, for frequencies below $0.1 \, \mathrm{m}^{-1}$, the measurement seems to indicate a sudden decrease of roughness. The measurement of the road height is compared to data from a high-resolution digital elevation model [29]. This DEM has a horizontal resolution of 0.5 m, and a vertical accuracy of approximately 10 cm. The strips of Belgian blocks are located on the DEM, and the resulting height profile is also visualised in Figure 7.

Several observations can be made from Figure 7. First, for the spatial frequency range from $0.04~\text{m}^{-1}$ to $0.2~\text{m}^{-1}$, the DEM and the measured road profile coincide well, indicating that both sources of information are in agreement. For spatial frequencies larger than $1/\lambda_2 = 0.2~\text{m}^{-1}$, the DEM seems to deviate from the measured road profile. The likely cause is that the road profile oscillations are nearing the accuracy limit of the DEM. Lastly, for frequencies below $1/\lambda_1 = 0.04~\text{m}^{-1}$, the DEM indicates that the road is of class B or

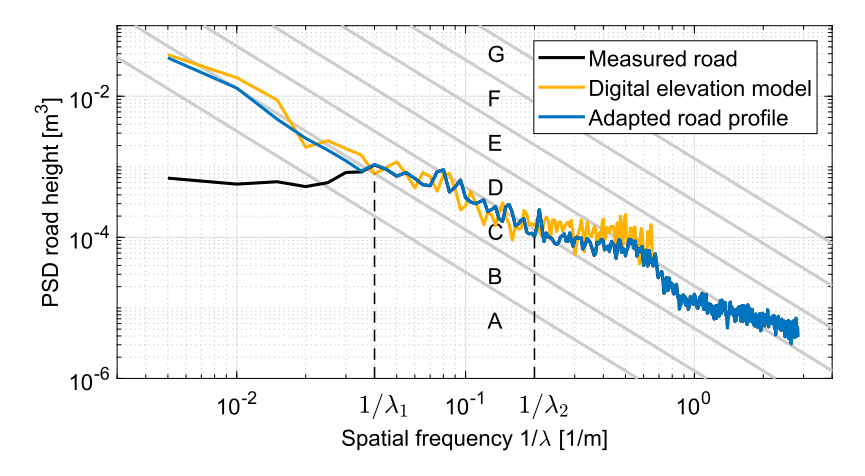


Figure 7. Power spectral density of the Belgian blocks, once based on measurements, once based on the elevation model, and the resulting adapted road profile. Road classes according to ISO 8608 are indicated as well.

C, whereas the measurement predicts barely any low-frequency oscillations. In this lower frequency range, the DEM is likely to be the more trustworthy source of information, as the measured road profile may have been filtered.

The measured road profile is adapted to construct a road input that is realistic over the entire frequency range. A synthetic random-road profile of road class B is generated. This profile is then low-pass filtered with a cut-off frequency of $1/\lambda_1 = 0.04 \, \text{m}^{-1}$, and the filtered signal is added to the measured road profile. The result is indicated in Figure 7 as well. For low frequencies, this signal has a similar energy content as the DEM, and for higher frequencies, it is equal to the measured road profile.

3.3.2. Results

The road profile, as described in Section 3.3.1, is used as input to the quarter-car model described in Section 2 with the vehicle parameters of Section 3.1. The simulated road input has similar spectral characteristics as the actual surface on which the vehicle was driven. Therefore, the frequency content of the simulation and measurement results can be directly compared.

Figure 8 shows the measurement and simulation results of an unladen vehicle traversing the Belgian blocks. The top figure displays the simulated road input as function of temporal frequency. The middle figure shows the estimated transfer function magnitude based on the input and output signals of the quarter-car model. Both the vehicle bounce eigenfrequency, around 1.3 Hz and the wheel hop eigenfrequency at 10 Hz are clearly visible. Lastly, the bottom figure in Figure 8 shows the Power Spectral Density (PSD), determined via Welch's method [30] of both the simulated suspension deflection and the measured suspension deflection signals. Measurements where performed at both the right and left wheels of the vehicle. Slight differences between these two are expected, as the left and right track of the road are not exactly equal. It can be seen that the simulated suspension deflection is in the same order of magnitude as the measured signals. This is also indicated by the power content of the simulation and measurement being roughly equal, as indicated

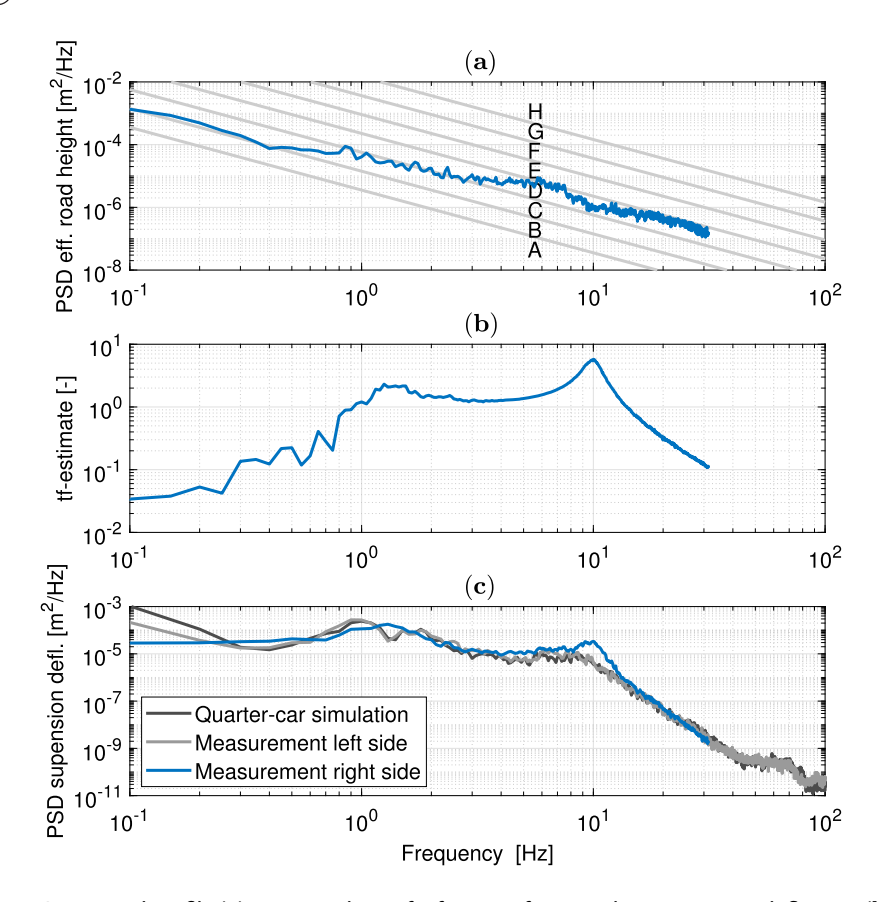


Figure 8. Input road profile (**a**), estimated transfer function from road to suspension deflection (**b**), and resulting suspension deflection (**c**) of an unladen vehicle at v = 40 km/h.

Table 3. Area under the PSD plots of the suspension deflection in Figures 8(c) and 9(c), indicating the total power content of each of the signals.

Loading	Meas. Left [m ²]	Meas. Right [m ²]	QC-simulation [m ²]
Unladen	2.01 · 10 ⁻²	1.74 · 10 ⁻²	1.68 · 10 ⁻²
Laden	2.00 · 10 ⁻²	1.83 · 10 ⁻²	1.94 · 10 ⁻²

in Table 3. Nevertheless, small differences are observed, for instance at the 10 Hz eigenfrequency. Here, the measurement data shows more damping than the model. A possible reason for this is that, for example, friction in the suspension, which is not modelled, results in additional damping. Alternatively, the possibility exists that the tyre damping coefficient in Table 1 is lower than the actual tyre damping. Furthermore, at frequencies below 0.3 Hz, the measurements show a larger output compared to the quarter car model, indicating that the very long wavelengths of $\lambda > 40$ m might be under-represented in modelled input.

Results of the Belgian blocks tests with a laden vehicle are displayed in Figure 9. These results are similar to those presented in Figure 8. The main difference is the vehicle bounce resonance peak, which shows a larger amplitude in the loaded vehicle situation. Because the air bellow stiffness changes according to (7), the frequency at which this peak occurs

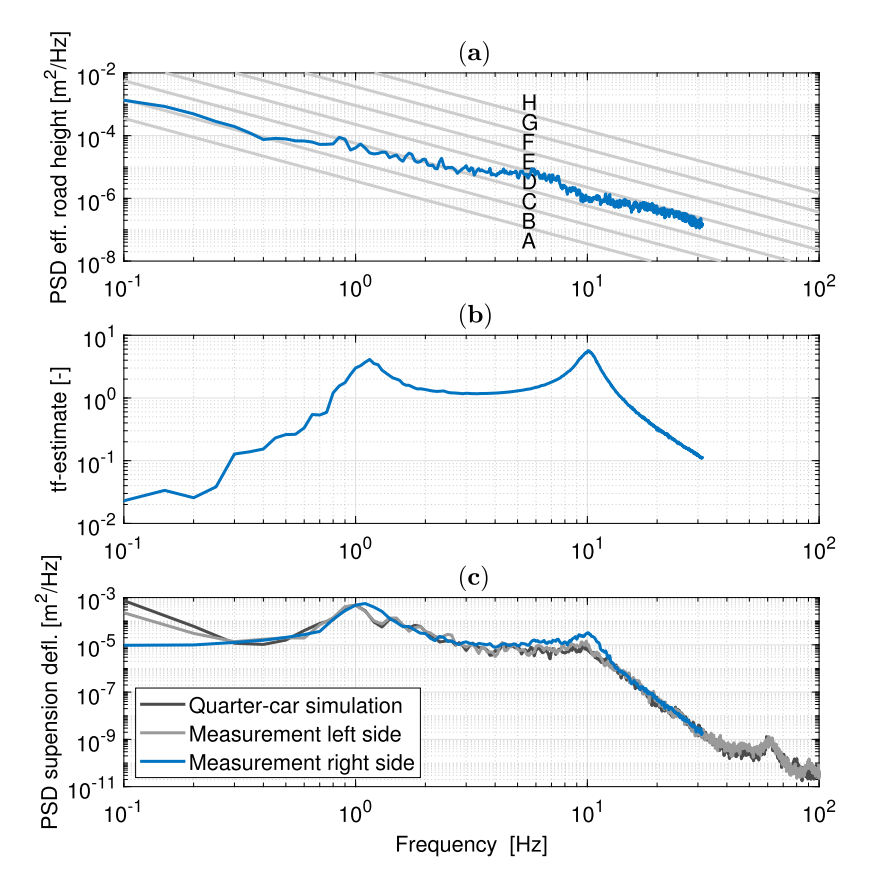


Figure 9. Input road profile (**a**), estimated transfer function from road to suspension deflection (**b**), and resulting suspension deflection (**c**) of an laden vehicle at v = 40 km/h.

barely changes between the two loading situations. Table 3 indicates the total signal power is comparable between model and measurement, and does not change heavily based on vehicle loading condition.

4. Quantification of damper losses

The quarter-car model that has been validated with measurement data of a diesel bus in Section 3 is used here to assess the energy dissipated in the dampers of a battery electric bus. The assumption is made that, if all physics-based model parameters are changed to those of a BEB, be model will describe reality equality well as in Section 3. These new battery electric bus parameters are described in Section 4.1. The results of the quarter-car model simulations are presented in Section 4.2 and compared to the results of coast-down tests in Section 4.3.

4.1. Vehicle parameters

The model parameters representing the battery electric bus are listed in Table 2. Separate sets of quarter-car-model parameters are used to represent both the front and rear axles of

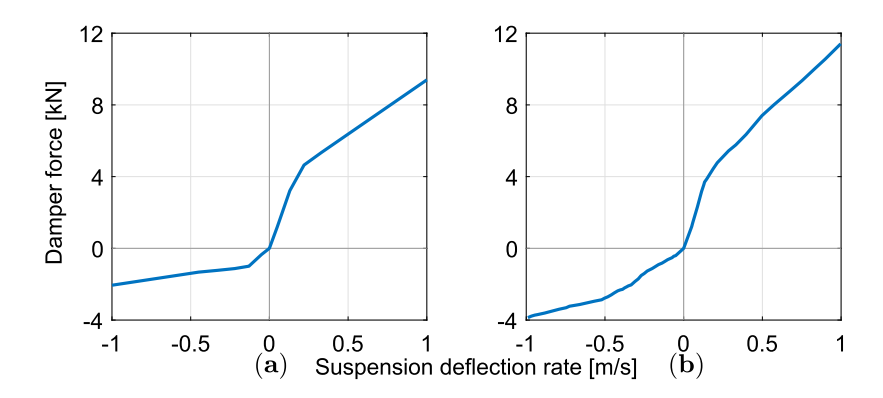


Figure 10. Damper force F_d versus damper deflection rate \dot{z}_s for both the front (**a**) and rear (**b**) suspension of the battery electric bus. The values represent the damping force per corner of the vehicle according to manufacturer specification.

the vehicle. By using this approach, the pitch dynamics of the vehicle and the wheelbase filtering effect are neglected. This is considered acceptable, because the pitch dynamics of a battery electric bus are generally slow due to the large moment of inertia, and the wheelbase filtering effect is shown to be less relevant for the suspension motion and dynamic tyre force [31]. The damper force characteristic for both axles is visualised in Figure 10. Again, two loading conditions are considered; an unladen vehicle and a laden vehicle.

With respect to the diesel vehicle in Section 3.1, the electric bus has a higher sprung mass and consequently a higher air bellow stiffness. The unsprung mass of the rear axle is slightly higher here because the rear axle here is driven and contains the final drive. Furthermore, the table shows the parameters for the front axle, which has only one air bellow, one damper, and one tyre per corner of the vehicle. The stiffness and damper characteristics presented in Figure 10 represent the effective values after accounting for suspension kinematics.

4.2. Random road input

As input to the simulation, random road profiles of classes A, B, C, and D will be considered. Higher road classes are of such poor quality that these are unlikely to be encountered by electric city buses. The resulting profiles are shown in Figure 11. Tyre enveloping is considered in the roads displayed in the figure according to the method described by Schmeitz [25]. This results in a dip in the frequency content of the road profiles, as the tyre envelops objects of this spatial dimension.

The quarter-car model with a nonlinear damper, as described in Section 3 is used to simulate the front and rear axle of the battery electric bus. The random-road profiles of Section 4.2 are used as input for these simulations.

For each road class A, B, C, and D, a 3 km section of road is simulated. The vehicle velocity is assumed to be constant at $\nu = 40$ km/h. The front and rear axle analyses are conducted independently with the same road profile. The effect of any coupling between the dynamics of the front and rear axle is thereby assumed to be small. The resulting energy dissipated per axle for both dampers and tyres is displayed in Figure 12.

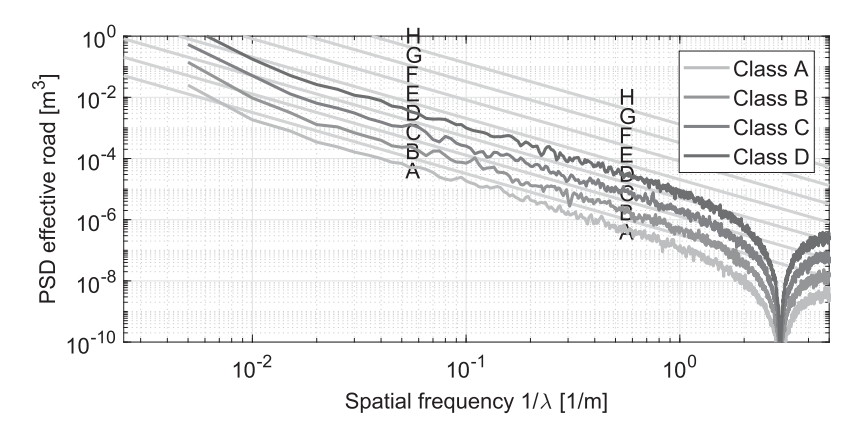


Figure 11. Power spectral density of the four effective random-road profiles used for the simulation study, each representing one road-roughness class.

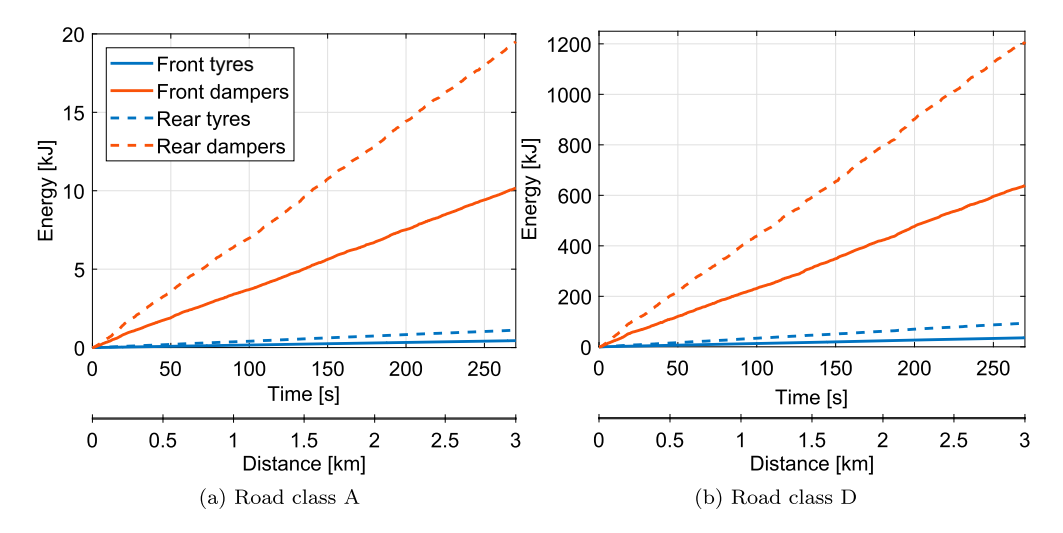


Figure 12. Simulated cumulative energy dissipated in dampers and tyres, indicated for both the front and rear axles for road classes A (**a**), and D (**b**). Results are for an unladen vehicle driving 40 km/h. (a) Road class A (b) Road class D.

The results for road class A, displayed in Figure 12(a), show that the total dissipated energy increases linearly with time. The dampers dissipate most of this energy, where the rear dampers dissipate almost twice as much energy as the dampers in the front suspension. This is in accordance with the fact that the rear axle is equipped with double springs, dampers, and tyres. By dividing the total dissipated energy by time, the front and rear dampers in this simulation dissipate 110 W combined on average. The dissipated energy increases with increasing road classes. Consequently, most energy is dissipated on the class D road, where all dampers combined account for 6.8 kW, as shown in Figure 12(b). Given that the vehicle has six dampers, this is approximately 1.1 kW per damper.

An overview of the average specific dissipated energy, expressed in kWh/km, is presented in Figure 13. The dissipated energy is partitioned into energy dissipated in the

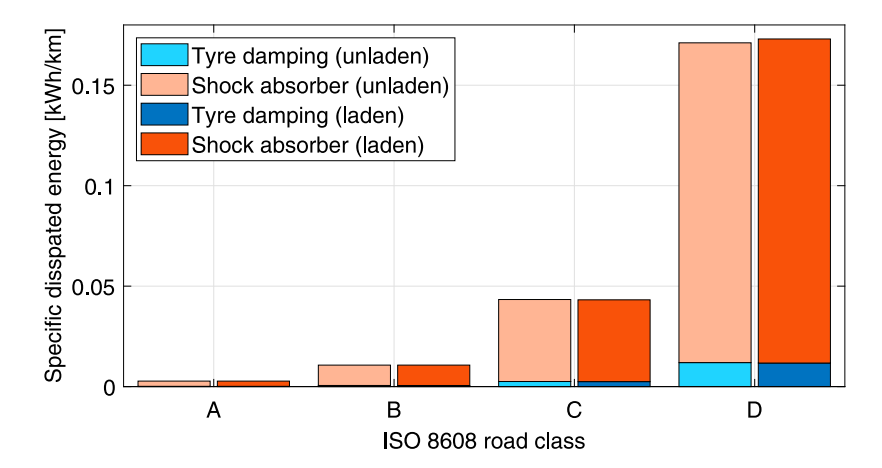


Figure 13. Total specific energy dissipated in the shock absorbers and tyres of a battery electric bus for different road classes. Results are shown for both an unladen and laden vehicle driving 40 km/h.

dampers and energy dissipated in the tyres. This shows that the contribution of tyre damping is relatively small. Data is shown for both a laden and an unladen vehicle. Surprisingly, the energy dissipated in the dampers in these two situations is very similar. This observation is likely a consequence of air bellow stiffness increasing with sprung mass, resulting in dynamics that are approximately mass-independent. Nevertheless, the literature suggests that even for vehicles with constant suspension stiffness, the dissipated damper energy mainly depends on tyre stiffness and is almost independent of other suspension parameters [13,32].

When comparing the different road classes, we see that the dissipated energy increases exponentially for increasing road classes. At $0.0027 \, \text{kWh/km}$, the total dissipated energy is lowest for road class A. For road class D, the total distance-specific energy amounts to $0.17 \, \text{kWh/km}$, which is approximately 13% of a representative energy consumption for a battery electric bus (= $1.3 \, \text{kWh/km}$), see [33, Figure 6].

The simulation results presented here are obtained at a simulated velocity of $40 \,\mathrm{km/h}$. Considering that the road PSD is effectively represented by a $-2 \,\mathrm{slope}$, as shown in Figure 11, and assuming that the constant velocity only affects the vertical tyre excision and no other vehicle dynamics, a doubling of the velocity is equivalent to increasing the road class by +1. In other words, the results presented for class B in Figure 13 would also represent the losses on a class C road at $20 \,\mathrm{km/h}$.

4.2.1. Frequency analysis

As previously shown in Figure 11, the random-road inputs have a broad frequency content that is representative of a realistic road. The question arises which frequency range is responsible for most of the energy consumption. To this end, the random-road profile is filtered with a low-pass filter of varying cut-off frequencies. These FIR filters are designed using the equiripple method from MATLAB's signal processing toolbox, with a stop band frequency of 2 times the cut-off frequency and a stop band attenuation of 10 dB and a pass band ripple of 0.05 dB. This results in a set of different road profiles that range from profiles with only low-frequency content to the original road profile with its full frequency content.

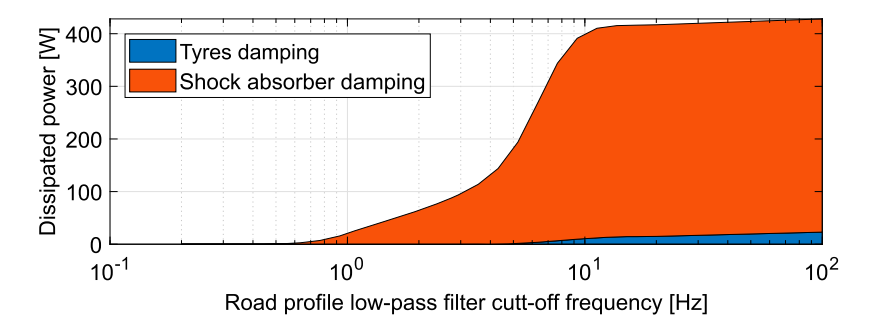


Figure 14. Dissipated power due to vertical damping in shock absorbers and tyres for different low-pass cut-off frequencies of the road profile. Simulation represents a BEB driving 40 km/h on a road of class B.

Each low-pass filtered profile is used as input to the quarter-car model representing the battery electric bus. The resulting dissipated energy is expressed, in Figure 14, where the original results are equivalent to those at the highest cut-off frequency of 100 Hz. The results show that the frequencies below 0.7 Hz do not contribute to the energy dissipation in the damper and tyre. The frequencies related to vehicle bounce, ranging from 0.7 to 3 Hz contribute 27% to the total dissipated energy. However, the majority of the energy, 73%, is dissipated due to road inputs in the 3 to 12 Hz frequency range. Only as of 7 Hz, tyre damping starts to become significant.

4.3. Coast-down tests

The dissipative damper losses described by the quarter-car model represent only part of the rolling resistance experienced by the bus. Energy is also dissipated due to hysteresis effects in the deformation of rubber in the tyre-road contact patch, micro-slip between tyre and road, and, in case of a wet road, due to displacement of water [3,34]. Because these effects are challenging to model based on first principles, the tyre rolling resistance is often measured on a drum test setup or through a vehicle test. In this case, the rolling resistance is determined from coast-down tests with a 12 m battery electric bus on various roads.

The coast-down tests are conducted in accordance with NEN-ISO 10521-1 [35]. During each test, the vehicle is accelerated to a certain speed, after which propulsion is removed, and the vehicle is allowed to slow down under the influence of rolling resistance and aero-dynamic resistance. By analyzing velocity as function of time, an estimate can be provided for both rolling resistance coefficient c_r and aerodynamic drag coefficient c_d . Measurements are repeated five times in both directions on each road to arrive at average values for both these parameters. The tests are conducted with an unladen vehicle on four different road surfaces: Smooth asphalt, standard asphalt, rough asphalt, and Belgian blocks. These four road surfaces correspond to the first classes of the random road profiles, respectively: A, B, C, and D.

In order to compare these results, the energy dissipated in the dampers E_{damp} and tyres E_{tyr} as described in (10), is determined for all i = 1, ..., 4 corners of the vehicle and scaled with the vehicle mass and travelled distance to arrive at a rolling resistance coefficient

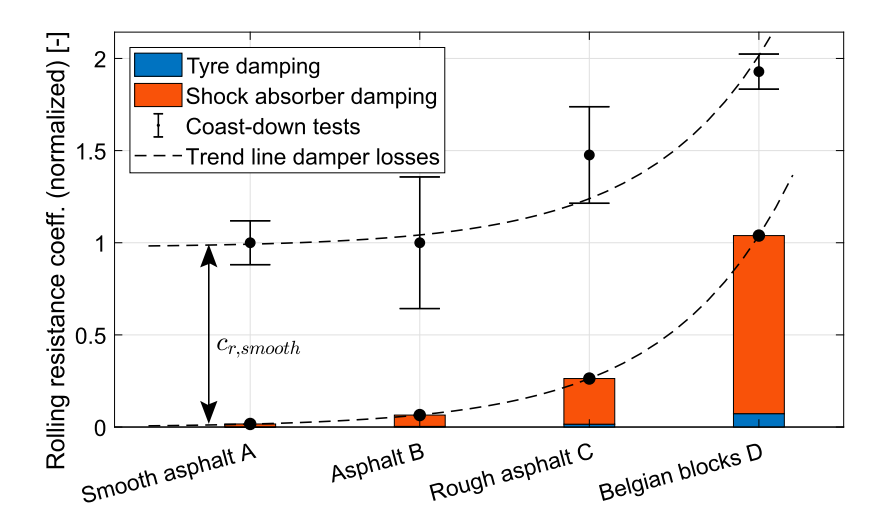


Figure 15. Tyre damping and shock-absorber damping expressed as rolling resistance coefficient contribution. The trend line indicates increasing damper losses and is shown once with and once without offset of $c_{r,smooth}$. The error bars indicate the maximum and minimum rolling resistance measured using coast-down tests.

contribution, respectively,

$$c_{r,damp} = \frac{\sum_{i=1}^{4} E_{damp,i}(t)}{m \, g \, v \, t} \qquad c_{r,tyr} = \frac{\sum_{i=1}^{4} E_{tyr,i}(t)}{m \, g \, v \, t}, \tag{14}$$

where *m* is the total vehicle mass. The resulting rolling resistance contributed both due to shock absorber losses and vertical tyre damping losses are shown in Figure 15. The results of the coast-down tests are shown as well, where the error bars indicate the maxima and minima of all parameter estimates.

The results in Figure 15 show that the rolling resistance obtained from coast-down tests approximately doubles when going from smooth asphalt to Belgian blocks. This rolling resistance can be perceived as the sum of the rolling resistance on a smooth surface, $c_{r,smooth}$, and the rolling resistance contributed due to shock absorber and tyre damping losses. The trend line in Figure 15 indicates that the road-roughness dependency of the coast-down test results and the damper losses predicted by the quarter-car model have a similar order of magnitude and trend. Therefore, it is concluded that the majority of the rolling resistance increase on rough roads is caused by energy dissipation in the dampers and, to a lesser extent, by energy dissipation in the tyres. Although it is acknowledged that the rolling resistance of a tyre on a smooth surface can increase for velocities above 100 km/h [34], the damper losses described here are the dominant reason for increasing resistance while increasing road roughness or increasing vehicle velocity.

The results presented in Figure 15 can further be placed into perspective through comparison to average BEB specifications. By assuming an average bus-tyre rolling resistance of 5.5 N/kN [3] and a tare vehicle weight as indicated in Table 2, the average rolling resistance force for an empty BEB is approximately 776 N. This corresponds to $776 \,\mathrm{Ws/m} =$ 0.215 kWh/km, which is approximately 16 % of the average consumption of 1.3 kWh/km



[33]. Figure 15 indicates a doubling of the rolling resistance could caused by rougher roads, which would signify an additional 16% increase in energy consumption.

The results presented in this work aim to split damper losses from the total rolling resistance. A further split of the remainder of the rolling resistance, including aerodynamic losses or slip losses, could be considered. An example is [14], where the energy lost due to longitudinal tyre slip is quantified and compared to the damper losses, and is found to be significant. The current model presented here assumes constant velocity and does not allow for a realistic quantification of slip losses.

5. Conclusion

The energy lost due to stroking of the suspension dampers when driving over road irregularities is quantified. A quarter-car model with nonlinear suspension dampers and tyres is validated based on data of an 18 m, three-axle city bus. Two known road inputs are used; a road bump and Belgian blocks. The simulated road bump compares well to measurements during compression and rebound, and the energy balance of the quarter-car model is demonstrated. The Belgian block simulations, performed with both a laden and an unladen vehicle, compare well to the measured suspension deflection in the frequency domain.

The validated model is employed to calculate the damper energy losses for a set of generated random-road profiles. For all these profiles, the energy dissipated in the rear axle is roughly twice as large as the energy in the front axle. The energy dissipated due to vertical damping of the tyre is one order of magnitude smaller than due to suspension damping. Using the validated model, the vertical dynamics can be directly linked to energy consumption, which is not often done. The road roughness significantly affects the total dissipated power, which can reach 6.8 kW, or 0.17 kWh/km, on roads of class D at 40 km/h. This corresponds to approximately 13% of the nominal energy consumption of a battery electric bus. These results are independent of vehicle mass due to the mass-dependent air bellow stiffness, which indicates that the results could be generally applicable to heavy-duty vehicles with air suspension of various weights. Comparing the results to rolling resistance coefficients determined from coast-down tests indicates that the effects described here are responsible for the majority of the road-surface dependency of the rolling resistance coefficient. Lastly, by low-pass filtering the road input, it is established that the road frequencies between 3 and 12 Hz constitute 70% of the dissipated energy.

Several improvements to this study are conceivable. Firstly, this work only concerns the losses attributed to the suspension dampers and the vertical damping of the tyre. If a complete first-principles rolling resistance model is desired, a model representing the hysteric tyre losses on a smooth surface should be added. Secondly, to more accurately simulate large vertical excitations of the suspension, the nonlinear thermodynamic effects of the compressed air in the bellows should be considered. Likewise, the inclusion of bumpand rebound stops might be considered. Furthermore, making the damper force positiondependent, $F_d = F_d(z_d, z_d)$, allows for the modelling of the hysteresis that is often present in shock absorbers [16]. Lastly, it remains an open topic to simulate the dissipated damper power in both front and rear axle and correlate these to the vehicle's powertrain power in the time domain. While the results presented here indicate a clear trend in average rolling resistance, making a rolling resistance force prediction for a particular road profile involves more detailed tyre and powertrain dynamics.



Disclosure statement

No potential conflict of interest was reported by the author(s).

Funding

This work was supported by the European Union's Horizon 2020 research and innovation programme under Grant No. 713771; This work was supported by the Horizon 2020 Framework Programme. The majority of this work was performed while the first author was employed at Eindhoven University of Technology.

References

- [1] IEA. Global ev outlook 2024. Paris: IEA; 2024.
- [2] Vepsäläinen J, Kivekäs K, Otto K, et al. Development and validation of energy demand uncertainty model for electric city buses. Transp Res Part D Transp Environ. 2018;63:347-361. doi: 10.1016/j.trd.2018.06.004
- [3] Bachmann CO. Vergleichende rollwiderstandsmessungen an lkw-reifen im labor und auf realen fahrbahnen [dissertation]. Aachen: RWTH Aachen University; 2017.
- [4] Miège AJP, Popov AA. Truck tyre modelling for rolling resistance calculations under a dynamic vertical load. Proc Inst Mech Eng Part D J Automob Eng. 2005;219(4):441-456. doi: 10.1243/095440705X11176
- [5] Gillespie TD, Sayers MW, Segel L. Calibration of response-type road roughness measuring systems. Washington, DC: Transportation Research Board, National Research Council; 1980.
- [6] Karnopp D. Power requirements for traversing uneven roadways. Veh Syst Dyn. 1978;7(3): 135-152. doi: 10.1080/00423117808968558
- [7] Velinsky SA, White RA. Vehicle energy dissipation due to road roughness. Veh Syst Dyn. 1980;9(6):359-384. doi: 10.1080/00423118008968630
- [8] Segel L, Lu X. Vehicular resistance to motion as influenced by road roughness and highway alignment. Aust Road Res. 1982;12(4):211-222.
- [9] Lu XP, Segel L. Vehicular energy losses associated with the traversal of an uneven road. Veh Syst Dyn. 1986;15(sup1):342-352. doi: 10.1080/00423118608969146
- [10] Lu XP, Segel L. Vehicular energy losses associated with the traversal of an uneven road. Veh Syst Dyn. 1985;14(1-3):166–171. doi: 10.1080/00423118508968823
- [11] Crolla DA, Abouel Nour AMA. Power losses in active and passive suspensions of off-road vehicles. J Terramech. 1992;29(1):83-93. doi: 10.1016/0022-4898(92)90016-D
- [12] Abdelkareem MAA, Xu L, Ali MKA, et al. Vibration energy harvesting in automotive suspension system: a detailed review. Appl Energy. 2018;229:672-699. doi: 10.1016/j.apenergy.2018. 08.030
- [13] Smith MC, Swift SJ. Power dissipation in automotive suspensions. Veh Syst Dyn. 2011;49(1-2):59-74. doi: 10.1080/00423110903427421
- [14] Wang JC, Wang FH, Wang YX, et al. Analysis of real-time energy losses of electric vehicle caused by non-stationary road irregularity. Energy. 2023;282:128444. doi: 10.1016/j.energy.2023.128444
- [15] Wallaschek J. Dynamics of non-linear automobile shock-absorbers. Int J Non Linear Mech. 1990;25(2-3):299-308. doi: 10.1016/0020-7462(90)90059-I
- [16] Surace C, Worden K, Tomlinson GR. On the non-linear characteristics of automotive shock absorbers. Proc Inst Mech Eng Part D J Automob Eng. 1992;206(1):3-16. doi: 10.1243/PIME_PROC_1992_206_156_02
- [17] Elliott SJ, Tehrani MG, Langley RS. Nonlinear damping and quasi-linear modelling. Philos Trans R Soc A Math Phys Eng Sci. 2015;373(2051):20140402. doi: 10.1098/rsta.2014.0402
- [18] Boere S, Arteaga IL, Kuijpers A, et al. Tyre/road interaction model for the prediction of road texture influence on rolling resistance. Int J Veh Des. 2014;65(2/3):202. doi: 10.1504/IJVD.2014.060815



- [19] Hoever C, Kropp W. A model for investigating the influence of road surface texture and tyre tread pattern on rolling resistance. J Sound Vib. 2015;351:161-176. doi: 10.1016/j.jsv.2015.04.009
- [20] Lundberg OE, Nordborg A, Lopez Arteaga I. The influence of surface roughness on the contact stiffness and the contact filter effect in nonlinear wheel-track interaction. I Sound Vib. 2016;366:429-446. doi: 10.1016/j.jsv.2015.12.026
- [21] Huang Y, Chen H. Review of rolling resistance influence on fuel consumption of trucks. In: 13th ITS Eur. Congr.; Brainport(Netherlands): ERTICO; 2019. p. 12.
- [22] Ejsmont JA, Ronowski G, Świeczko-Żurek B, et al. Road texture influence on tyre rolling resistance. Road Mater Pavement Des. 2017;18(1):181-198. doi: 10.1080/14680629.2016.1160835
- [23] Svenson G, Fjeld D. The impact of road geometry and surface roughness on fuel consumption of logging trucks. Scand J For Res. 2016;31(5):526-536. doi: 10.1080/02827581.2015.1092574
- [24] Rill G. Road vehicle dynamics. Boca Raton: CRC Press; 2011. (Ground vehicle engineering
- [25] Schmeitz AJC. A semi-empirical three-dimensional model of the pneumatic tyre rolling over arbitrarily uneven road surfaces [dissertation]. Delft: TU Delft; 2004.
- [26] Mathworks. Solver [Available from: https://nl.mathworks.com/help/simulink/gui/solver. html]; 2022. [accessed 2022-02-03].
- [27] Johannesson P, Rychlik I. Modelling of road profiles using roughness indicators. Int J Veh Des. 2014;66(4):317. doi: 10.1504/IJVD.2014.066068
- [28] ISO 8608:2016. Mechanical vibration road surface profiles reporting of measured data. Delft(Netherlands): Koninklijk Nederlands Normalisatie-instituut; 2016.
- [29] Algemeen Hoogtebestand Nederland. AHN.nl [Available from: https://www.ahn.nl/]; 2021. (accessed on 27 November 2021).
- [30] Welch P. The use of fast fourier transform for the estimation of power spectra: a method based on time averaging over short, modified periodograms. IEEE Trans Audio Electroacoust. 1967;15(2):70-73. doi: 10.1109/TAU.1967.1161901
- [31] Song K, Chen X, Lin Y. Wheelbase filtering effect on vehicle ride dynamics. In: Proceedings of the FISITA 2012 World Automotive Congress; Berlin, Heidelberg: Springer Berlin Heidelberg; 2013. p. 1183-1195.
- [32] Botshekan M, Tootkaboni MP, Louhghalam A. Global sensitivity of roughness-induced fuel consumption to road surface parameters and car dynamic characteristics. Transp Res Rec. 2019;2673(2):183–193. doi: 10.1177/0361198118821318
- [33] Beckers CJJ, Besselink IJM, Nijmeijer H. The state-of-the-art of battery electric city buses. In: 34th Int. Electr. Veh. Symp. Exhib.; Nanjing(China): 2021. p. 8.
- [34] Michelin. The tyre rolling resistance and fuel savings. Clermont-Ferrand: Sociéte de Technologie Michelin; 2003.
- [35] ISO 10521-1:2006. Road vehicles road load part 1: determination under reference atmospheric conditions. Delft(Netherlands): Nederlands Normalisatie-instituut; 2006.